AIAA JOURNAL
Vol. 40, No. 7, July 2002

Active Flow Separation Control on Wall-Mounted Hump at High Reynolds Numbers

Avi Seifert*
Tel-Aviv University, 69978 Ramat Aviv, Israel
and
LaTunia G. Pack†
NASA Langley Research Center, Hampton, Virginia 23681

An active separation control experiment was conducted in a cryogenic pressurized wind tunnel on a wall-mounted bump at chord Reynolds numbers from 2.4×10^6 to 26×10^6 and a Mach number of 0.25. The model simulates the upper surface of a 20% thick Glauert–Goldschmied-type airfoil at zero incidence. The turbulent boundary layer of the tunnel sidewall flows over the model and eliminates laminar–turbulent transition from the problem. Indeed, the Reynolds number either based on the chord or boundary-layer thickness had a negligible effect on the flow and its control. Without control, a large turbulent separation bubble is formed at the lee side of the model. Periodic excitation and steady suction or blowing were applied to eliminate gradually the separation bubble. Detailed effects due to variations in the excitation frequency, amplitude, and the steady mass flux are described and compared to those of steady suction or blowing. It was found that the amplitude of the most effective frequency for separation control is rapidly attenuated in the reattachment region. The superposition of weak steady suction enhances the receptivity of the separated shear layer to the fundamental excitation frequency and, therefore, the effectiveness of the periodic excitation, whereas weak steady blowing promotes the generation of higher harmonics and reduces the excitation effectiveness. Separation control using periodic excitation and weak suction are similar in both effectiveness and dynamics, whereas steady blowing generates steadier flow but is of inferior effectiveness and is abrupt in nature and is, therefore, not suitable for closed-loop control. The data set enhances the understanding of active separation control at high Reynolds numbers and is a proper validation case for unsteady numerical design tools.

Nomenclature

C_{dp} = pressure drag coefficient
C_m = quarter-chord moment coefficient
C_n = normal force coefficient
C_p = wall pressure coefficient, $(P - P_s)/q$
C_{pt} = total pressure coefficient, $(P_t - P_s)/q$
C_μ = combined momentum coefficient, $(c_\mu; \langle c_\mu \rangle)$
c = model reference chord
c_μ = steady mass transfer momentum coefficient, J/cq
$\langle c_\mu \rangle$ = excitation momentum coefficient, $\langle J' \rangle/cq$
F^+ = reduced frequency, $(f^* x_{sep})/U_\infty$
f = excitation frequency, Hz
h = slot height or width
J = momentum at slot exit, $\rho h U_j^2$
LN_2 = liquid nitrogen
M = Mach number
P = pressure
q = freestream dynamic pressure, $1/2\rho U_\infty^2$
R_c = chord Reynolds number, $U_\infty c/\nu$
R_θ = momentum thickness Re number
T = temperature
U, u = average and fluctuating velocity
x/c = normalized streamwise location
x_{sep} = distance from separation to reattachment
y = distance normal to wall
z = spanwise location
ν = kinematic viscosity
ρ = density

Subscripts

d = derectified hot-wire data
R = reattachment
sp = separation
∞ = freestream conditions

Superscripts

2D = two-dimensional
$'$ = root mean square of fluctuating value

Presented as Paper 99-3403 at the AIAA 30th Fluid Dynamics Conference, Norfolk, VA, 28 June–1 July 1999; received 17 April 2001; revision received 21 November 2001; accepted for publication 2 January 2002.

*Senior Lecturer, Department of Fluid Mechanics and Heat Transfer, Faculty of Engineering; also Visiting Scientist, Institute for Computer Applications in Science and Engineering, NASA Langley Research Center, Hampton, VA 23681; seifert@eng.tau.ac.il. Associate Fellow AIAA.

†Research Engineer, Flow Physics and Control Branch. Member AIAA.

I. Introduction

THE realization of thick, efficient fluid dynamic shapes is limited by boundary-layer separation. In 1904, Prandtl applied slot suction to delay flow separation from a circular cylinder (see Ref. 1). Criteria were developed[2,3] for obtaining the strongest turbulent adverse pressure gradient without separation and applied[4] to design efficient high-lift airfoils. Several ideal flow methods were developed[5–7] for designing airfoils with a long fetch of laminar flow, followed by a severe adverse pressure gradient and a suction slot to prevent boundary-layer separation. The Glauert–Glas II airfoil (see Refs. 6 and 8) was wind-tunnel tested and flight proven.[9] The approach was applied[10] to bodies of revolution and integrated with the propulsion and boundary-layer control (BLC) systems.

Many factors prevented widespread utilization of laboratory proven BLC techniques such as blowing or suction: low efficiency, complexity, and maintainability, to count a few. Forced oscillations superposed on a mean flow that is on the verge of separating were

found to be very effective in delaying turbulent boundary-layer separation.[11] Experiments performed on various airfoils at low and high Reynolds numbers[12–14] demonstrated that, even if the flow is not fully attached, the lift can be increased by periodically exciting the separated shear layer. This is achieved by introducing frequencies that generate 2–4 spanwise coherent vortices over the length of the separated region, that is, $F^+ \approx 1$ (Ref. 13). The addition of periodic excitation into a separating turbulent boundary layer increases the momentum transfer across the shear layer, enhancing its resistance to separation. Though demonstrated experimentally, unsteady separation control is still a challenge for numerical simulation, and design tools are missing.

At least two approaches could be considered for an aerodynamic design process that includes active BLC. One is to attempt improving the performance of an existing geometry, that is, fixes, using experience and experiments. The second is to integrate unsteady BLC into a multidisciplinary optimization design process. This should allow simplified high-lift systems, thicker airfoils that will allow lighter structures and greater internal volume, shorter aft bodies, size reduction, and even elimination of conventional control surfaces. Existing design tools are capable of reproducing steady flows, including steady mass transfer, but the inclusion of unsteady BLC effects into computational fluid dynamics (CFD) tools has not been performed. The development of a proper CFD design tool is dependent on the availability of a comprehensive database to allow its validation.

The present paper describes an experiment aimed at improving our understanding of controlling separated flows at flight Reynolds numbers and providing a comprehensive database for validation of unsteady CFD design tools. The suction surface of a modified Glauert–Glas II airfoil (see Refs. 6 and 8) is currently tested. The thickness to chord ratio of the airfoil was reduced to 20%, and periodic excitation replaces the suction that was used to keep the boundary layer attached. Laminar–turbulent transition, which eludes quantitative comparison between experiment and computation, for example, high-lift flows,[15] has been excluded from the problem because the model boundary layer is turbulent throughout. The thickness of the incoming turbulent boundary layer was adjustable. The boundary layer on the model and the mean and fluctuating wall pressures were measured. The two dimensionality of the wall pressures was verified. BLC using steady blowing or suction was compared to periodic excitation.

II. Description of the Experiment

A. Hump Model

The model simulates the upper surface of a 20% thick variant of the Glauert–Glas II airfoil (see Ref. 6) (Fig. 1). Without control, the flow separates at $x/c \approx 0.66$. A suction slot (or several slots) was used on a similar airfoil and axisymmetric shapes to eliminate the separation and even generate pressure (or form) thrust.[9,16] Presently, periodic excitation and steady suction and blowing are used to reattach the separated flow. The model is installed on the tunnel right-side turntable. The model cavity is easily accessible for the introduction of spanwise uniform pressure fluctuations (Figs. 1 and 2). The turbulent boundary layer on the tunnel sidewall flows over the model, its thickness is monitored by a traversed probe

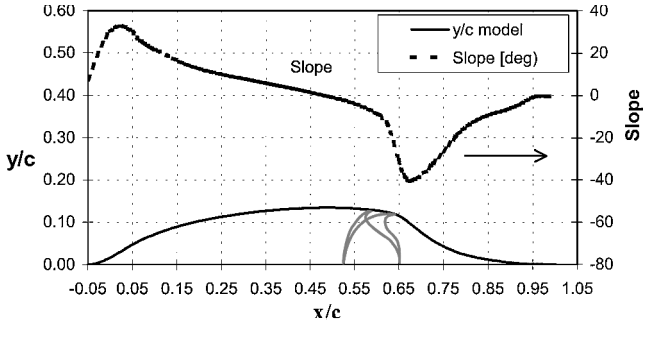

Fig. 1 Cross section of the hump model, showing the alternative slots at $x/c = 0.59$ and $x/c = 0.64$, actuator cavity and surface slope.

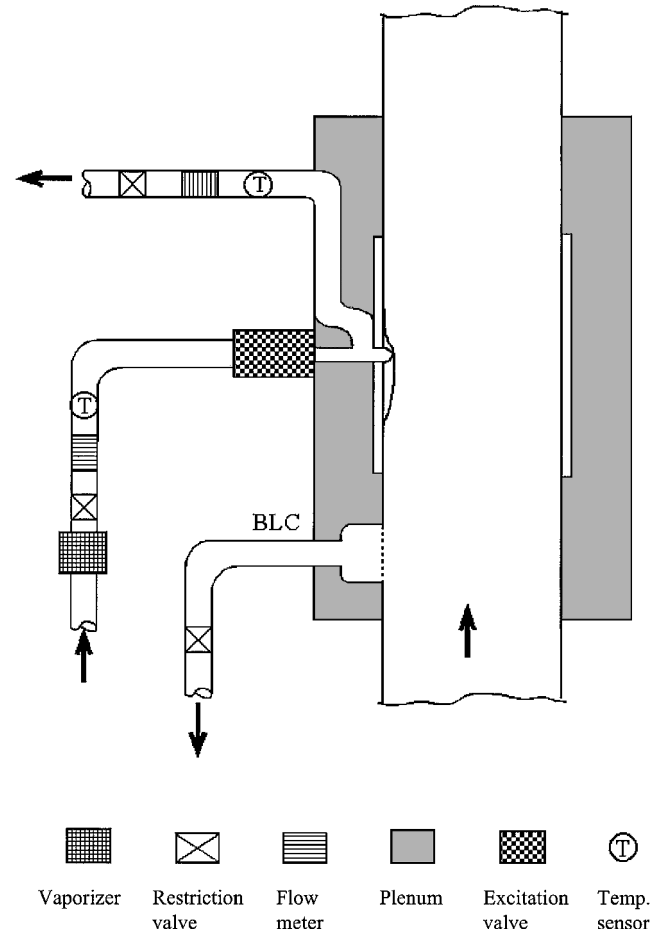

Fig. 2 Top view of the experimental setup in the NASA 0.3-Meter Transonic Cryogenic Tunnel; model is shown on the left-side turntable.

and adjusted by a sidewall boundary-layer removal system. Several differences between the present arrangement and airfoil flow could be noted. The primary ones are the existence of a reattachment region at all flow conditions and the lack of unsteady interaction between the lower and upper surface flows at the trailing edge and in the wake.

The model reference chord is 200 mm. The original location of the airfoil leading edge is defined as the reference leading edge, $x/c = 0$ (Fig. 1). This area was faired smoothly between $x/c = -0.05$ and 0.05 to eliminate a slope discontinuity and local separation. Two alternative blowing slots are available: $x/c = 0.59$ and 0.64 (both shown in Fig. 1). The position of the upstream slot was selected such that it would be upstream of the expected position of a shock wave.[17,18] The slots were 0.25% chords wide (0.50 mm ±10%) and were inclined at 30 deg to the surface facing downstream (Fig. 1). The tunnel floor and ceiling boundary layers are not affecting the spanwise uniformity of the flow over the model due to the use of a pair of end plates (see the thick vertical lines in Fig. 3). A gap of 12.7 mm between the end plates and the tunnel walls was deemed sufficient, based on the available wind-tunnel boundary-layer data.[19] Additional data acquired during this experiment verified this. The tunnel cross-sectional blockage due to the model and the end plates was 0.0836. The model was equipped with one streamwise and three spanwise rows of pressure taps (Fig. 3). The model was also instrumented with 12 dynamic pressure transducers (indicated by × symbols in Fig. 3). The transducers were installed under the model surface, inside small volume cavities. One transducer was flush mounted near the trailing edge of the turntable next to a recessed pressure transducer, and their readings are compared. Another dynamic pressure transducer is installed inside the model cavity, midway between the end plates and about 30 mm from the slot exit. It was used to monitor the cavity pressure oscillations and to correlate the wind-tunnel experiments with the bench-top tests.

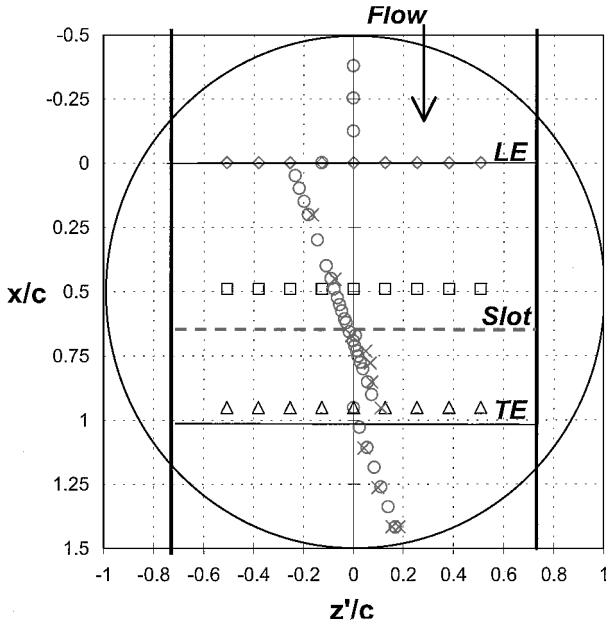

Fig. 3 Elevation view of the model showing streamwise (circles) and the three rows of spanwise pressure taps (diamonds, squares, and triangles), the dynamic pressure sensors (×), the excitation slot at $x/c = 0.64$, and the end plates (vertical thick lines).

B. NASA 0.3-Meter Transonic Cryogenic Wind Tunnel

The experiment was conducted in a transonic cryogenic wind tunnel. It is a closed-loop, fan-driven tunnel with a test cross section of 0.33×0.33 m (Refs. 20 and 21). An automatic control system maintains the test conditions, providing a high level of repeatability. The floor and ceiling of the tunnel were slightly diverged near the model to reduce blockage resulting from boundary-layer growth on the test-section walls. The tunnel sidewalls are parallel. The pressures on the wall opposite the model were measured to evaluate wall interference.

The tunnel boundary-layer removal (BLC) system consists of a pair of porous plates located between 451 and 273 mm upstream of the turntable centers and spans the tunnel height (BLC in Fig. 2). The streamwise extent of the porous plates is 178 mm. The mass flow rate through the right-side boundary-layer removal system was not measured, but the boundary-layer thickness upstream of the model was measured at all test conditions. Only the right-side BLC system, that is, that of the model (Fig. 2), was used.

C. Periodic Excitation System

A rotating, siren-type valve was used to generate the pressure oscillations inside the model cavity. The oscillatory blowing valve was capable of generating frequencies up to 800 Hz. A pressure regulator was used to control the gaseous nitrogen (GN_2) entering the valve, and the variable speed drive of the valve motor was used to control the frequency. The oscillatory blowing valve was attached to the right tunnel plenum door (Fig. 2). The outlet of the oscillatory blowing valve was connected to the backside of the model cavity. Suction ports were positioned at the entrance to the model cavity. These ports were connected to the unused left-side tunnel boundary-layer removal system. The digital valves of the left-side boundary-layer removal system were used to control the steady flow rate out the suction ports (Fig. 2). Steady suction or steady blowing was applied to the model flow by holding the oscillatory blowing valve in the fully open position and varying the inlet or the exhaust mass flow rates.

D. Boundary-Layer Measurement System

A total pressure probe with an internal tip diameter of 0.25 mm was used to measure the boundary layer. The probe penetrated the flow side of the model through slots in the turntable. It was mounted on a two-dimensional traversing system, located on the backside of the turntable. The slots were sealed by a ribbon-cage mechanism that allows travel along the turntable surface. The position resolution was $\pm 2.5 \times 10^{-5}$ mm, but the wall position was only known to within ± 0.1 mm. The x and z locations had a similar uncertainty. The data were always acquired when the probe traveled away from the wall.

E. Instrumentation

The model surface pressures were measured at 60 locations. Normal force, moment, and form drag were calculated from these measurements. Volume flow rates were combined with temperature and pressure measurements to determine the mass flux entering and exiting the model cavity (see Fig. 2). The mean mass flux in or out of the excitation slot could be determined by subtracting these two mass fluxes. A dynamic pressure transducer, flush mounted in the model cavity, measured the pressure fluctuations produced by the oscillatory valve. The cavity temperature and the tunnel static pressure were used to calculate the GN_2 density in the cavity.

F. Bench-Top Experiments

The velocity fluctuations at the excitation slot were measured with the model outside the tunnel using hot wires. The GN_2 was replaced with air. The wind-tunnel and the bench-top experiments were otherwise similar. In the cases where reverse flow was encountered at the slot exit, the hot-wire signal was derectified.[22] The cavity dynamic pressure and hot-wire velocity were acquired using a 16-bit high speed A/D converter, coupled with an antialiasing filter.

The frequency response of the model surface dynamic pressure transducers was modified due to small differences in the installation of individual transducers. To evaluate this effect, all of the transducers underwent a bench-top calibration. A sound source and a microphone were placed as close as possible to each installed transducer, and the frequency range of interest was covered. The results presented here are only for the flat range of the transducers' frequency response that cover at least twice the highest excitation frequency used in the test.

G. Experimental Uncertainty

Most of the experiments were conducted at conditions close to the limits of the wind-tunnel operating envelope. For example, the very low temperatures (about 100 K), and Mach numbers are close to the lower limit of the tunnel capability. Most of the data were obtained with separated flow regions on the model. Table 1 contains the relevant information regarding experimental uncertainties. These values were calculated using ± 3 standard deviations of the various experimental conditions and calculated parameters (including repeated runs).

The uncertainty of the calculated aerodynamic parameters is listed in Table 2 (in absolute values and related to flow condition on the model).

The experiments reported here were conducted at a Mach number of 0.25 and chord Reynolds numbers ranging from 2.4×10^6 to 26×10^6.

Table 1 Uncertainty of flow and control parameters[a]

Item	Uncertainty, % of full scale	Full scale and condition
LN_2 line pressure	2	150 psi
Slot width	10	0.5 mm
Static temperature	0.3	300 K
Static pressure	0.25	77 psi
R_c	1	$M > 0.2$
M	2	$M < 0.3$
F^+	2	2
c_μ	0.01 or 10%	Larger
$\langle c_\mu \rangle$	25	Local values
f	0.3	800 Hz
U hot wire	1.5	Local values
u'_d	15	Local values
x/c of BL data	0.5	% chord
Wall position	0.1 mm	——
p'	0.4	10 psid
x, y, z	0.01 mm	Bench top

[a]Percent of full scale unless otherwise noted.

Table 2 Uncertainty of aerodynamic parameters

Parameter	Baseline	Controlled
C_n	0.010	0.015
C_{dp}	0.0005	0.0010
C_m	0.005	0.010

III. Results

The first subsection in the results section describes the bench-top calibration, aimed at correlating the slot exit velocities with the cavity pressure fluctuations. The second subsection describes the baseline flow over the model. The third subsection describes the controlled flow. Effects of the upstream boundary-layer thickness, the Reynolds number, the excitation frequency and its magnitude, and the effect of steady mass transfer alone or superimposed on the excitation are all considered.

A. Bench-Top Calibration of the Excitation Slot

A bench-top calibration was performed to correlate the fluctuating slot velocities u'_d with the cavity pressure fluctuations p'. The squared fluctuating slot exit velocities u'^2_d for the high-amplitude range[14] are plotted in Fig. 4a vs p'/ρ for all of the frequencies of the $x/c = 0.59$ slot. The root mean square deviation of the data points around the linear fit is about 25% (based on local values). The frequency response of the present excitation system (oscillatory blowing valve–manifold–cavity) is significantly simpler than the one used previously.[14] The dynamic pressure transducer is now installed inside the cavity (at about half the cavity span and about 30 mm from the slot exit), and the pressure fluctuations are introduced in a spanwise uniform manner (Fig. 2). The u'_d for the low-amplitude range are presented in Fig. 4b. Again, the data follow the linear fit, in accordance with the appropriate scaling.[14] The collapse of the data for the two amplitude ranges (separated at $u'_d \approx 13$ m/s), regardless of the forcing frequency, allows us to generate a single correlation between u'_d and p'/ρ for each slot. The correlation for the high-amplitude range ($p'/\rho > 450$) of the $x/c = 0.59$ slot data is

$$u'^2_d = 1.088p'/\rho - 280 \tag{1}$$

For the low-amplitude range ($p'/\rho < 450$) the correlation is

$$u'_d = 0.0325p'/\rho \tag{2}$$

The slope of this line is lower than the slope of the linear fit to the data presented in Fig. 4b, that is, 0.036, but was selected such that the calibration would contain a smooth transition between the low- and high-amplitude ranges around $p'/\rho = 450$. Reducing the slope of the low-amplitude fit is justified because the slot velocity derectification process tends to increase u'_d at the low-amplitude range (Ref. 22; Fig. 7) for zero mass flux excitation.

A similar procedure was performed for the $x/c = 0.64$ slot calibration data. The correlations for that slot are

$$u'^2_d = 1.173p'/\rho - 246 \qquad \text{for} \qquad p'/\rho > 375 \tag{3}$$

$$u'_d = 0.0372p'/\rho \qquad \text{for} \qquad p'/\rho < 375 \tag{4}$$

The small difference in the calibration curves for the two slots results from a small difference in the slot geometry (see Fig. 1). Because of the modular nature of the model, the slot width changed by ±10% (0.005 mm) between runs. Cryogenic cycling could also have a similar effect on the slot width, and this is accounted for in the uncertainty level of $\langle c_\mu \rangle$, that is, ±25%.

Whereas these measurements were made at the slot half-span, measurements were also made from the slot center to one end plate at a frequency of 780 Hz, the highest used in the test, where the possible nonuniformity should be the highest due to the short wavelength. It was found that the slot exit velocities do not vary by more that ±2.1%, and the corresponding spanwise phase distribution was uniform (±5 deg).

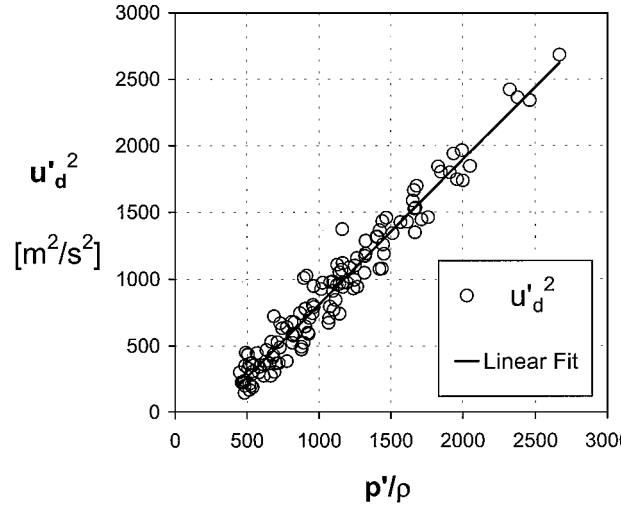

a) High-amplitude range

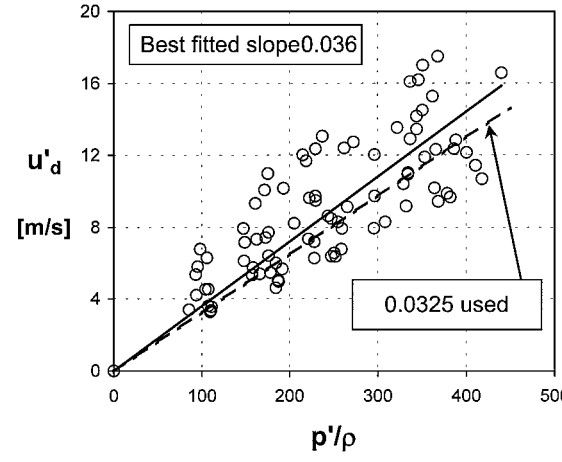

b) Low-amplitude range

Fig. 4 Derectified fluctuating slot exit velocities vs cavity pressure fluctuations from the bench-top experiment ($x/c = 0.59$ slot).

B. Description of the Baseline Flow

1. Effect of the Reynolds Number

The Reynolds number has a weak effect on the flow over the model, presumably because laminar–turbulent transition was eliminated from the problem. Figure 5 shows the model baseline mean (solid lines) and fluctuating (broken lines, right-hand side ordinate) pressures for $R_c = 2.4 \times 10^6$–26×10^6 at $M = 0.25$. The flow at the model reference leading edge (LE) (note that only $x/c > 0.2$ is shown in Fig. 5) decelerates to generate a partial stagnation point.[23] The flow rapidly accelerates on the first 15% of the chord, then the acceleration decreases up to $x/c = 0.5$, where the suction peak is located. The small step in C_P at $x/c \sim 0.45$ is a result of a breakline in the model, and the smaller step at $R_c = 2.4 \times 10^6$ indicates that it might be enhanced by uneven thermal stresses at cryogenic conditions. A pressure recovery starts at $x/c = 0.55$ and persists until $x/c = 0.65$, where the flow separates. The vertical broken line in Fig. 5 indicates the slot location. The surface slope at the separation area is about 40 deg (Fig. 1), and the curvature changes sign there. The separation location is fixed, regardless of the Reynolds number. It is not affected by the location of the blowing slot or by the interaction of the external flow with the cavity.[23] Weak Reynolds numbers effects, such as a small increase in the flow acceleration at $x/c = 0.4$ and a small increase in C'_p, that is, larger C'_p at separation, and smaller C'_p at reattachment, are noted (Fig. 5). The initial separation height above the reference plane, that is, tunnel wall, is $y/c = 0.115$, the model thickness at separation.

A large turbulent separation bubble is formed at the lee side of the model. The flow above the bubble initially accelerates, indicating a spreading of the mixing layer. The separated mixing layer starts to interact with the surface and turns toward it at

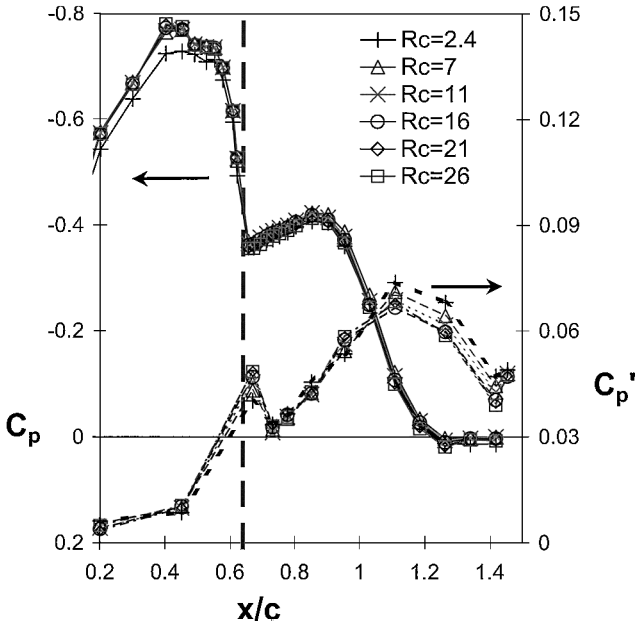

Fig. 5 Mean (solid lines) and fluctuating (broken lines) wall pressures at $M = 0.25$; Reynolds numbers in millions; dashed vertical line indicates $x/c = 0.64$ slot.

$x/c > 0.9$, reattaching at $x/c \approx 1.2$. On a complete airfoil, under similar flow conditions, reattachment would not occur, and an open reverse flow region would interact with the wake. The bubble in the present setup is closed because the model is installed on the tunnel wall.

The level of the pressure fluctuations upstream of separation is very low (Fig. 5). A significant increase in the level of C'_p is noted immediately downstream of separation ($x/c > 0.65$). Just upstream of reattachment ($x/c \approx 1.1$) the level of the pressure fluctuations peaks due to the intermittent nature of the reattachment process and the associated unsteady stagnation point close to the surface. Several numerical and experimental investigations established that the peak in the wall pressure fluctuations occurs about one separation height upstream of reattachment (Fig. 3 in Ref. 24 and references therein). The mean reattachment location is assumed to be $0.115c$ downstream of $C'_{p,\max}$, that is, one initial separation height. The reattachment region closely corresponds to the region where $C_p \approx 0$, downstream of the separation point. Reattachment of the baseline flow, as determined by the preceding criteria, occurs at $x/c = 1.21 \pm 0.05$ for all of the incompressible Reynolds numbers studied. A small but consistent elongation of the bubble length as the Reynolds numbers decrease was found. The length of the baseline bubble is, therefore, $x_{\text{sep}}/c = x_R - x_{\text{sp}} = 0.57 \pm 0.03$. However, in the definition of F^+, x_{sep} was assumed to be $c/2$.

The integral aerodynamic parameters acting on the model at $M = 0.25$ are $C_n = 0.43 \pm 0.01$, $C_{\text{dp}} = 0.0268 \pm 0.0005$, and $C_m = -0.174 \pm 0.005$, regardless of the Reynolds number. These parameters were calculated using all of the pressure taps in the range $-0.4 < x/c < 1.45$. A small, but distinctive, decrease in the normal force and in the form drag were measured as the Reynolds number was increased. The normal force coefficient C_n is not a good indicator of the success of the control method on this configuration. Because of the large separation bubble, the normal force decreases as the size of the controlled bubble decreases. This occurs because the flow cannot turn down after it leaves the trailing edge (TE) and the flow deceleration region at the LE can not move to the lower surface as a stagnation point would on an airfoil. The form drag C_{dp} and the moment about the quarter chord C_m are the prime indicators because they are better correlated to the level of the excitation and behave in a similar manner to airfoil flow parameters. Moreover, the fixed boundary conditions upstream and downstream of the model, regardless of the level of flow attachment on the lee side of the model, will significantly simplify the computational effort of future numerical simulations.

The spanwise uniformity of the model C_p is ± 0.011 around its mean at $x/c = 0$ and at $x/c = 0.49$ and ± 0.003 at $x/c = 0.95$, that is, the spanwise uniformity of C_p over the lee side of the bubble is almost perfect. The path of the streamwise pressure taps (shown in Fig. 3) is in the range $-0.25 < z/c < 0.2$, well within the range of the uniform spanwise pressure distribution. The pressure distributions on the tunnel wall opposite the model were also measured to evaluate wall interference effects. The interference at $M = 0.25$ is very weak, with a $C_{p,\min}$ on the opposite wall of -0.12.

The spectral content of the model surface pressure fluctuations (not shown) contains a broad peak centered on $F^+ = 0.8$ at $x/c = 0.7$. The lower frequency range of the spectra fills very rapidly with the x direction over the separation bubble. At reattachment, the spectra show a broad peak centered on $F^+ = 0.4$. Detailed analysis of the flowfield dynamics was presented in Ref. 25.

2. *Effect of the Upstream Boundary-Layer Thickness*

The thickness of the upstream boundary layer has a minor effect on the flow over the model. Even though the momentum thickness of the upstream boundary layer was halved, only minor changes were observed in the steady and fluctuating model pressures. The boundary layer on the tunnel sidewall upstream of the model, at $x/c = -1.25$, was measured (Fig. 2). The measured velocity profiles were all fully developed and turbulent with the universal slope of the law of the wall, but lower offset due to the somewhat rough tunnel wall and porous plate.[19,23] The effect of the Reynolds number is to reduce the boundary-layer thickness gradually.[23] The momentum thickness of the upstream boundary layer is about 0.6% of the model reference chord. The relative thickness of the boundary layer to the chord length θ/c is one of the parameters affecting the flow development over the model. Corresponding θ/c on the TE of the main element of high-lift systems[15] at takeoff conditions are about 0.2% for $R_c = 9 \times 10^6$ and $M = 0.2$. The variation in the baseline boundary-layer thickness parameters is about 20% over the very wide range of high Reynolds numbers studied, having a negligible effect on the current model pressures and integral parameters. The shape factors H of the boundary layers at $M = 0.25$ are $H = 1.27 \pm 0.01$ over the R_c range (Fig. 6).

The momentum thickness Reynolds number of the incoming boundary layer R_θ (Fig. 6) is often used to characterize viscous effects on the flow. The range of Reynolds number R_θ covered in the present experiment is from 0.47×10^5 to 1.49×10^5. The tunnel boundary-layer removal system was used to thin the boundary layer upstream of the model to simulate a wider range of R_θ and θ/c. Figure 7 shows that θ could be reduced by 43%, simulating much higher chord Reynolds numbers and reducing R_θ. The two ways to obtain the same R_θ (i.e., by varying θ or U_∞) makes this parameter an inadequate candidate for describing the evolution of the flow over the model. Indeed, the effects of reducing θ by 43% are to decelerate the flow upstream of the model (as expected in higher Reynolds number R_c), slightly delay separation, and slightly move the reattachment point upstream. The effect on C'_p is negligible (not shown;

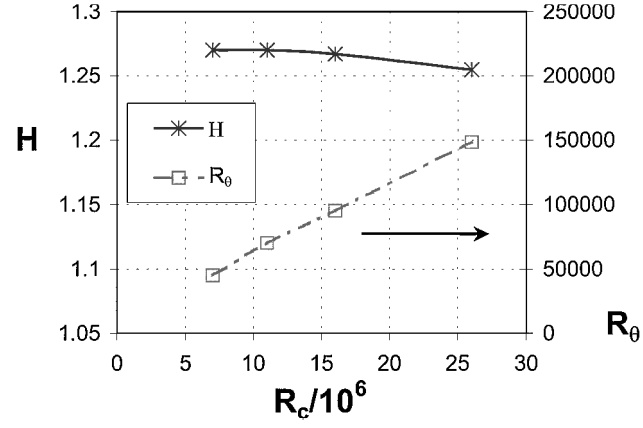

Fig. 6 Boundary-layer shape factor and momentum thickness Reynolds number at $M = 0.25$; data were acquired at $x = -1.25c$.

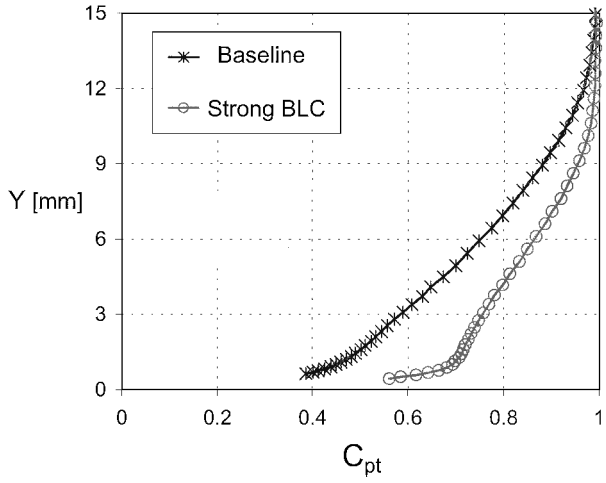

Fig. 7 Mean velocity profiles of the baseline and with strong BLC: $x/c = -1.25$, $M = 0.25$, and $R_c = 7 \times 10^6$.

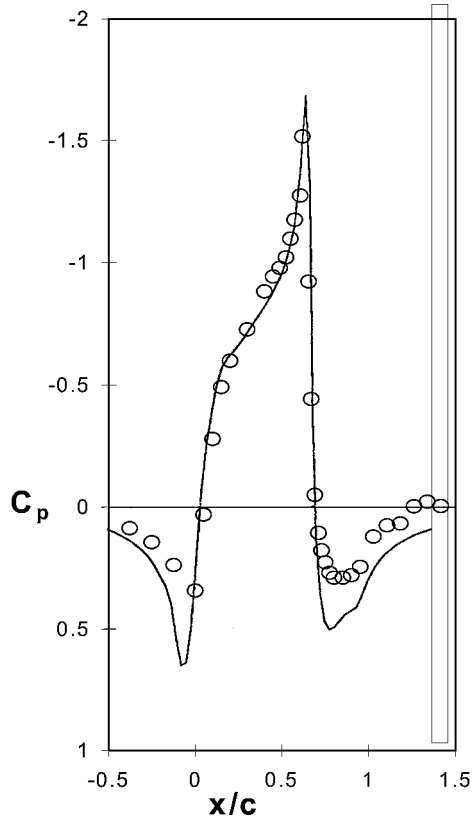

Fig. 8 Experimental model pressures due to suction $c_\mu = 4\%$ (symbols) compared with ideal pressure distribution (solid line).

see Ref. 23). It is suggested that Reynolds number R_c and θ/c are the suitable parameters to describe the viscous effect on the flow over the model. We conclude that the effect of the upstream boundary-layer thickness on the separation and subsequent reattachment is small, as long as transition does not occur close to separation.

The effect of controlling the flow separation at the lee side of the model, on the boundary layer upstream of the model, was also investigated. This was performed by fully attaching the flow to the model using slot suction with $c_\mu = 4 \pm 1\%$ (Fig. 8) and also by using the strongest available periodic excitation, with $F^+ = 0.8$ and $\langle c_\mu \rangle = 0.55\%$ (not shown). The large uncertainty level of the steady c_μ is due to the large pressure drop across the slot that increases the uncertainty in the calculation of the cavity density. The effect of the model separation control on the upstream boundary layer was negligible. (Its thickness decreased by less than 1%.) The strong periodic excitation had a small effect on the steadiness of the upstream boundary layer at the measuring station. It increased C'_{pt} inside the boundary layer by 10%, and outside the boundary layer it generated C'_{pt} that is from four to five times higher than the freestream turbulence level. The minute effect of controlling the model separation on the upstream boundary layer leads to the conclusion that the upstream boundary layer is not affected by the model separation control, within the experimental uncertainty. This will allow a numerical simulation to keep the upstream boundary condition unchanged, regardless of the flow conditions on the model.

C. Controlled Flow over the Hump Model

1. Effect of the Upstream Boundary-Layer Thickness

There is no attached baseline flow for comparison with the actively controlled flow because the baseline flow contains a separation bubble. Therefore, steady suction or blowing was applied to reattach the flow fully, and it is compared to ideal flow computations. An example of the attached flow due to steady suction with $c_\mu = 4\%$ is presented in Fig. 8. The agreement between the measured and calculated pressure distributions is very good, indicating that the theoretical prediction that led to the design of the original Glauert airfoil[6] (see also Ref. 5) has been reproduced successfully. The small differences are attributed to the existence of boundary layers on the model and to the exclusion of the slot from the calculation grid.

The Reynolds number has a weak effect on the effectiveness of the periodic excitation. As seen before in airfoil experiments[14,17] and in the present baseline flow, the Reynolds number has a minor effect on the flow characteristics, presumably because laminar–turbulent transition was eliminated from the problem. The effect of the upstream boundary-layer thickness on the controlled flow over the model is small, as it was for the baseline flow (Fig. 9). This effect was tested at $R_c = 7 \times 10^6$, where the boundary-layer thickness is relatively large. Identical excitation was applied with and without removing boundary-layer fluid through the BLC system. The upstream boundary-layer conditions were identical to those presented in Fig. 7. The flow deceleration upstream of the model increases due to the thinner boundary layer ($x/c < 0.2$, not shown in Fig. 9). From $x/c = 0$ to separation, and almost to reattachment ($x/c \approx 1$), the two pressure distributions are identical. Only downstream of reattachment are the mean pressures higher when the upstream boundary layer is thinner. The slight increase in C'_p due to the thinner boundary layer is expected because the flow receptivity to the excitation partly relies on the shear across the excitation slot. Indeed, the shear across the slot increased as the boundary layer becomes thinner (boundary-layer data, not shown). We conclude that the thickness of the upstream boundary layer has little effect on the controlled as well as the baseline flow over the model.

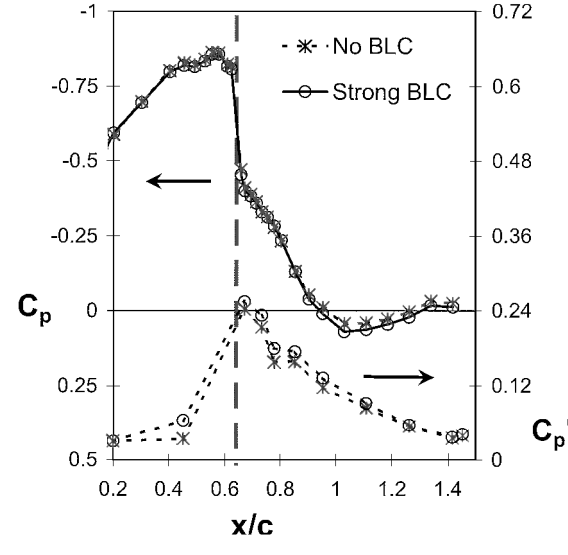

Fig. 9 Mean and fluctuating model pressures showing the effect of upstream BL thinning: $R_c = 7 \times 10^6$, $M = 0.25$, $F^+ = 1.15$, $\langle c_\mu \rangle = 0.16\%$, slot $x/c = 0.64$, and BLC as in Fig. 7.

2. Effect of the Excitation Frequency

It was previously shown that the effective excitation frequency scales with the length of the separated region and is inversely proportional to the freestream velocity.[13] The mechanism responsible for this observation is not fully understood. It is assumed that the upper limit of the effective frequencies is the Kelvin–Helmholtz instability of the separated shear layer. The lower limit of the effective frequencies is of the same order as the natural shedding frequency of the baseline configuration. Note that clean, stationary vortex shedding was not identified at high-Reynolds-number turbulent flows,[14] nor was it found on the present configuration. A feedback loop between the periodic excitation, applied at the separation point, and the reattaching flow that transmits pressure fluctuations upstream, is presumably active. Therefore, the flow could be considered globally unstable and, therefore, sensitive to both upstream and downstream boundary conditions. The control methodology is further complicated because the length of the separated region decreases as the excitation becomes more effective, increasing the effective frequencies. However, this last trend is favorable because the high-amplitude slot excitation generates higher harmonics even if the excitation signal in the model cavity is purely monotonic.[25] The length of the separated region was presently taken as half of the chord length and the range of the available excitation frequencies allowed the generation of reduced frequencies in the range $F^+ = 0.2$–2.0.

The mean and fluctuating model pressures for low excitation amplitude of $\langle c_\mu \rangle = 0.03\%$ are presented in Fig. 10. The length of the bubble was reduced by 35% using excitation frequencies that generate $F^+ > 0.4$. The control reduced C_p both upstream and downstream of the slot. The fluctuating model pressures (Fig. 10), reveal that the peak in the model pressure fluctuations $C_{p,\max}$ moves forward as the excitation frequency increases, indicating a forward motion of the reattachment point. Also note that the C_p' for $F^+ = 0.4$ and 0.8 are amplified downstream of the slot. Furthermore, due to the longer wavelengths that the lower F^+ generate, and the overall higher level of unsteadiness, a strong C_p' was measured at $x/c = 0.2$ and 0.45. As the excitation frequency increases, this upstream effect diminishes. The amplitude at the excitation slot is essentially fixed for $F^+ > 0.4$ and peaks at $x/c = 0.67$. (Data at $F^+ = 1.2$ and 2.0 were excluded for clarity.) The secondary C_p' peak is attributed to controlled reattachment. If F^+ is to be modified according to the length of the controlled separated region, it should decrease by about 35%.

Figure 10 also presents steady suction data at the same C_μ as the periodic excitation. The suction pressure distribution is similar to that of $F^+ = 0.4$. Note that the application of steady suction moves the reattachment point forward, but also increases the level of C_p' in a similar manner to the high F^+ unsteady excitation (Fig. 10).

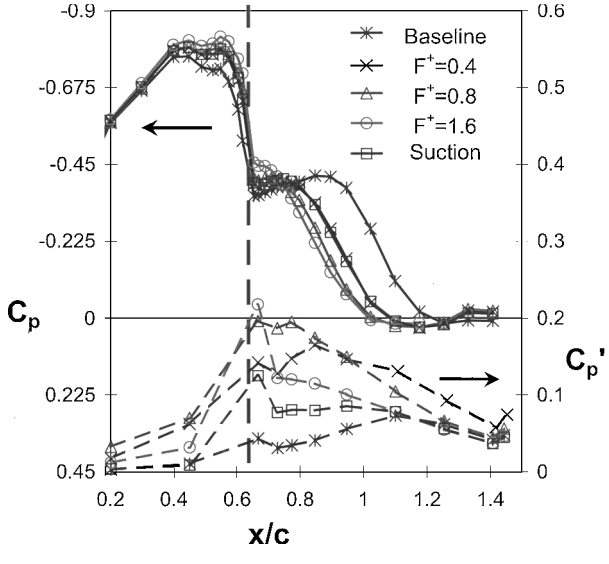

Fig. 10 Mean and fluctuating model pressures showing the effect of the excitation frequency and steady suction: $C_\mu = 0.03\%$, $R_c = 16 \times 10^6$, $M = 0.25$; vertical dashed line indicates $x/c = 0.64$ excitation slot.

Therefore, it is concluded that any forward motion of the reattachment point is associated with a higher level of C_p' at a more forward location, as long as separation was not completely eliminated.

Note that $F^+ = 1.6$ is most effective in increasing the suction level upstream of the slot and in generating a healthier pressure recovery downstream of it (Fig. 10). However, the data also show that the pressure rise across the slot increases only from 0.15 in the baseline to 0.26 for the $F^+ = 1.6$ data. The purpose of using steady suction in the original Glauert[6] approach was to generate a localized pressure jump, whereas the advantage of periodic excitation is the unstable nature of the shear layer that amplifies the excitation. The challenge is to achieve significant control authority immediately downstream of the slot and not to rely on convective amplification. When the flow is turned absolutely unstable, it might be possible to increase the effectiveness of periodic excitation for controlling localized severe adverse pressure gradients. Physical insight resulting from global instability analysis should also be sought.

Figure 11a presents the effect of the excitation frequency at $\langle c_\mu \rangle = 0.13\%$. The effect of the increased amplitude (compared to Fig. 10) is to further shorten the separation bubble, at all frequencies used, with $F^+ = 1.6$ being the optimal. The C_p' distribution, also shown in Fig. 11a, is similar to that seen for the lower $\langle c_\mu \rangle$ (Fig. 10). One exception is that the level of the C_p' decreases below the level of the baseline C_p' for $x/c > 1.2$ and $F^+ \geq 0.8$.

The first step in gaining physical understanding about the dynamics of the control process is to study the evolution of the fundamental excitation frequency. Figure 11b presents the streamwise distribution of the wall pressure fluctuations at the excitation frequency for several F^+ that were presented in Fig. 11a. In the aforementioned data, the excitation signal is not a perfect sine wave; however, at least 90% of the cavity pressure fluctuation's power was at the fundamental, even though the pressure sensor at $x/c = 0.67$, immediately downstream of the slot, indicates a significantly higher

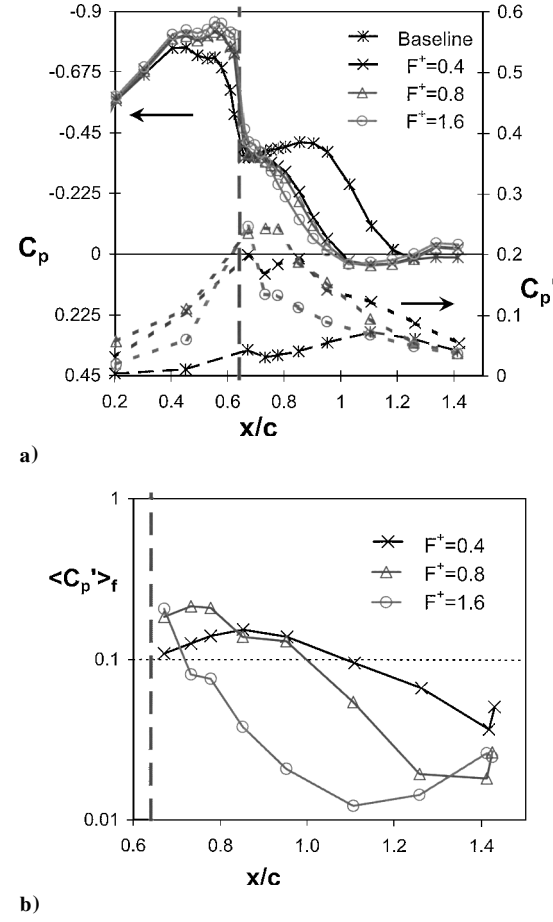

Fig. 11 Mean and fluctuating pressures showing the effect of a) excitation frequency and b) evolution of the pressure fluctuations at the fundamental frequency downstream of the $x/c = 0.64$ slot (vertical dashed line): $\langle c_\mu \rangle = 0.13\%$, $R_c = 16 \times 10^6$, and $M = 0.25$.

harmonic content than in the cavity. The separated shear layer is most receptive to $F^+ \approx 1$ and is less receptive to $F^+ = 0.4$ (Fig. 11b), but both this frequency and $F^+ = 0.8$ are amplified over the bubble. Whereas $F^+ = 0.8$ saturates at $x/c = 0.75$, $F^+ = 0.4$ continues to be amplified until $x/c = 0.85$. The separated flow is most receptive to $F^+ = 1.6$, which is the most effective frequency for reattaching the flow, but the C_p' amplitude at $F^+ = 1.6$ significantly decays as reattachment is approached, that is, at $x/c \approx 1$ according to Fig. 11a. Note that C_p' of $F^+ = 1.6$ is amplified downstream of reattachment ($x/c > 1.1$). The farthest downstream C_p' plotted in Fig. 11b ($x/c = 1.43$) was measured by the flush-mounted pressure transducer, and its reading and that of the recessed transducer next to it ($x/c = 1.42$) give an indication of the uncertainty level, that is, ±20%. Based on the data presented in Fig. 11b, it is concluded that the most effective frequency for separation control, that is, $F^+ = 1.6$, alters the mean flow through unsteady excitation, but the unsteadiness associated with it decays very rapidly. On the other hand, lower frequencies that are less effective in altering the mean flow continue to be amplified over the bubble and decay at a lower rate downstream of reattachment.

3. *Effect of the Excitation Amplitude*

The effect of increasing the excitation level at $F^+ = 1.6$ is presented in Fig. 12. The dashed vertical line at $x/c = 0.64$ indicates the excitation slot. It is shown that the bubble length decreases, even with $\langle c_\mu \rangle$ as small as 0.02%. An examination of the near slot region indicates that for $\langle c_\mu \rangle \leq 0.03\%$, the C_p at the slot area is shifted up, and only at $x/c \approx 0.8$ (Fig. 12) is the mixing rate high enough to start turning the flow toward the wall. The suction peak upstream of the slot became stronger, and the pressure recovery downstream of it is more favorable. Although the level of the cavity pressure fluctuations steadily increased, the corresponding C_p' at $x/c = 0.67$ saturated for $\langle c_\mu \rangle$ between 0.05 and 0.1%. This is an indication that the receptivity of the separated shear layer is limited and cannot be further exploited. The increased upstream effect as $\langle c_\mu \rangle$ increases occurs even though C_p' at the slot saturates. The relative improvement in performance with increasing $\langle c_\mu \rangle$ is rapidly decaying for $\langle c_\mu \rangle > 0.03\%$. However, it is clear that such a small $\langle c_\mu \rangle$ is insufficient to promote complete flow reattachment to the tested geometry.

4. *Effects of Steady Mass Flux*

It was previously shown[12–14,22] that the addition of steady mass flux, superimposed on the periodic excitation, is beneficial when separation occurs farther downstream of the excitation slot and the surface curvature is small. It is well known that changing the shape of the mean velocity profile affects the stability of the shear layer. The velocity profile turns absolutely unstable[26] for suction levels that generate reverse flow with about 30% of the local freestream velocity. On the present geometry, where a steep adverse pressure gradient starts slightly upstream of the excitation slot, it is crucial for the effectiveness of the periodic excitation to increase the flow receptivity to the imposed oscillations.

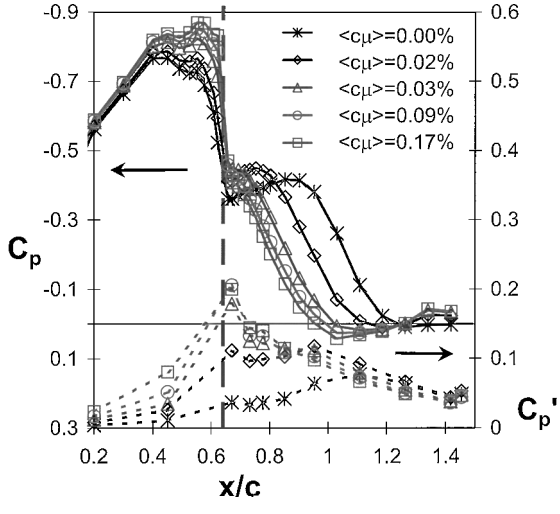

Fig. 12 Mean and fluctuating model pressures showing the effect of the excitation amplitude at $F^+ = 1.6$: $R_c = 16 \times 10^6$, $M = 0.25$, and $x/c = 0.64$ slot.

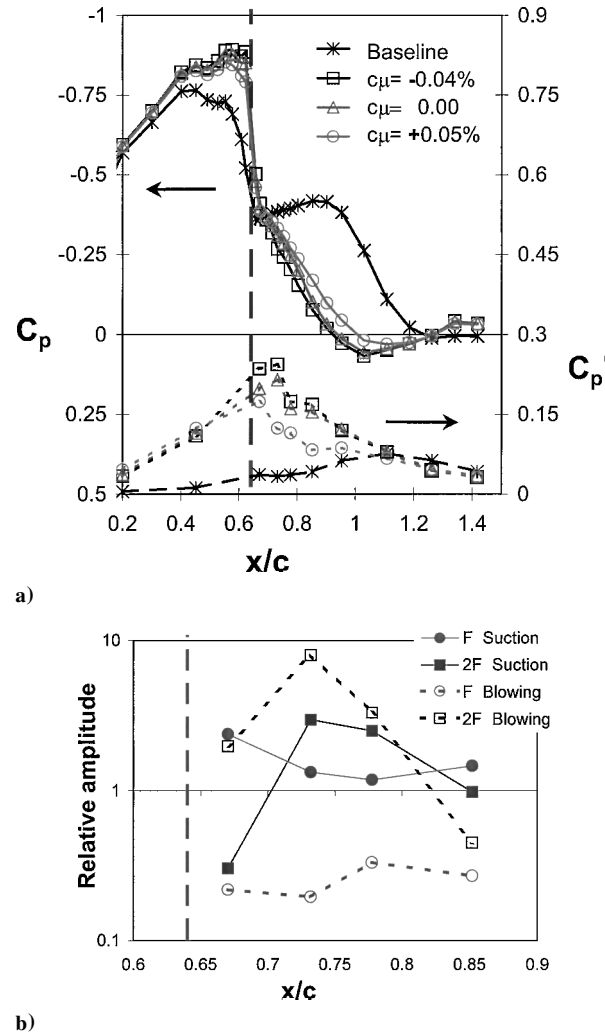

Fig. 13 Mean and fluctuating model pressures showing a) effect of superimposed weak steady mass flux on the excitation signal and b) effect of the added mass flux on the fundamental and its harmonic downstream of the slot: $R_c = 16 \times 10^6$, $M = 0.25$, $\langle c_\mu \rangle = 0.23\%$, $F^+ = 1.5$, and $x/c = 0.64$ slot.

Effects of weak suction or blowing superimposed on the periodic excitation on the wall pressures are shown in Fig. 13a. Weak suction increases the mean pressure recovery as well as the level of C_p' that is generated by the excitation, whereas weak blowing generates the opposite effect (Fig. 13a). The estimated magnitude of the slot suction velocity is 30% of the freestream velocity. The dynamic effects of the superimposed steady mass flux were analyzed by calculating the relative power spectral density of C_p' at integer multiples of the excitation frequency (F^+ and $2F^+$ are considered in Fig. 13b) and normalizing it by the power spectra of the corresponding frequency components generated by the zero mass flux excitation ($c_\mu = 0.0$). The relative power spectral densities for $0.67 < x/c < 0.85$ are plotted in Fig. 13b for F^+ and $2F^+$. The superimposed steady mass flux does not change the level and the spectral distribution of the cavity pressure fluctuations; therefore, $\langle c_\mu \rangle$ is unaffected. Whereas, for $c_\mu = 0$, comparable amplitudes are generated for the fundamental and its two first higher harmonics (as measured at $x/c = 0.67$, not shown), suction almost doubles the power of the fundamental, whereas blowing sends most of the excitation power to its harmonic. Note that the instability characteristics of the separated shear layer were not significantly altered by the superimposed mass flux. The separated shear layer amplifies $2F^+$ in a comparable manner, whereas F^+ is roughly neutral. The drastic change in the dynamics of the controlled flow are indicative of the great sensitivity of the receptivity process to changes in the

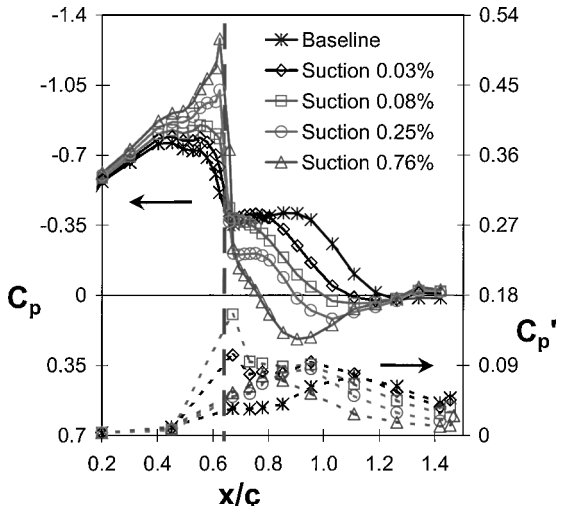

Fig. 14 Mean and fluctuating model pressures showing the effect of the steady suction: $R_c = 16\times10^6$, $M = 0.25$, $\langle c_\mu \rangle = 0.00\%$, $F^+ = 0.0$, and $x/c = 0.64$ slot.

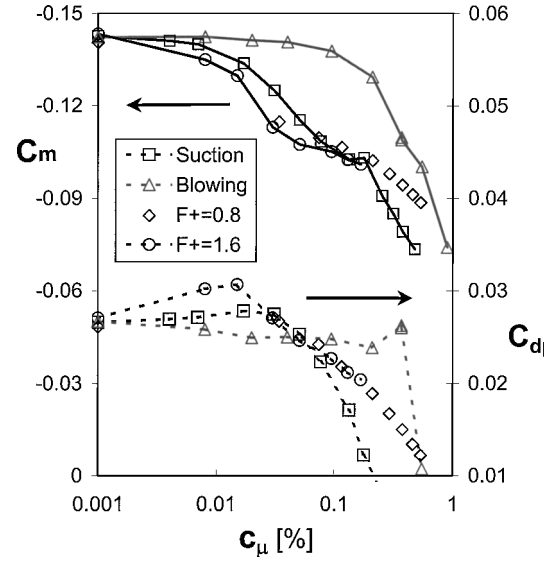

Fig. 15 Model quarter-chord moment and form drag coefficients due to steady suction, steady blowing, and periodic excitation at two frequencies: $R_c = 16\times10^6$, $M = 0.25$, and $x/c = 0.64$ slot.

boundary conditions by BLC, whereas the averaged wall pressures (Fig. 13a) show relatively little difference due to the changes in c_μ, presumably due to the high $\langle c_\mu \rangle$ used. The reproduction of these dynamic effects and further physical clarification are a challenge for numerical simulation and also require additional experimentation.

Steady suction or blowing alone, that is, $\langle c_\mu \rangle = 0$, were used to reattach the flow to provide a comparison between the effectiveness and characteristics of steady and unsteady BLC methods. The flow can be fully reattached to the surface of the model using either steady blowing or suction with $c_\mu \approx 2$ to 4%. Similar suction magnitudes were used by Glauert et al.[8] Steady blowing is ineffective at momentum coefficients less than 1%. It is possible to generate pressure thrust on the current model for steady mass flux above $c_\mu \approx 1\%$ due to the presence of a high-pressure region on the highly sloped aft body.[23] Figure 14 presents the steady and fluctuating wall pressures due to the application of steady suction. The effects of suction with $c_\mu \leq 0.15\%$ are similar to those of periodic excitation at comparable $\langle c_\mu \rangle$, as seen in Fig. 10. The bubble shortens and the location of $C'_{p,\max}$ moves upstream when steady suction is applied (Fig. 14). Note that the C'_p at $x/c = 0.67$ increases significantly due to be applied suction at $c_\mu < 0.18\%$. (The experiment was done at a finer suction level resolution than that presented in Fig. 14.) For $c_\mu > 0.18\%$, the pressure jump across the slot increases, C_p becomes more positive than the baseline downstream of the slot, and C'_p at $x/c = 0.67$ is much lower than the secondary $C'_{p\,\max}$ (positioned at $x/c = 0.95$ for $c_\mu = 0.25\%$), indicating that reattachment progressively moves upstream as c_μ increases and that enhanced mixing due to suction induced unsteady excitation is no longer active.

5. Summary of Control Effectiveness

The model integral parameters due to the application of steady suction, steady blowing, and periodic excitation are presented in Fig. 15. The form drag C_{dp} is initially increased due to periodic excitation and suction, but for $C_\mu > 0.02\%$, it gradually decreases. The form drag was eliminated for suction $c_\mu \approx 0.8\%$ and blowing $c_\mu \approx 2\%$. Form thrust is generated at higher levels of steady mass transfer (not shown). Steady blowing is significantly less effective in reattaching the flow than suction on the current geometry. The quarter-chord moment starts to respond only at blowing $c_\mu > 0.1\%$, and the form drag does not change for blowing $c_\mu < 0.5\%$. In addition to the lower control authority, the steplike response of the aerodynamic parameters to steady blowing is not desirable for control purposes. It is further shown (Fig. 15) that periodic excitation is significantly more effective than steady blowing and at least comparable to steady suction at $C_\mu < 0.1\%$. The C_m is more sensitive to oscillatory excitation than to steady suction and significantly less sensitive to steady blowing. Only at $c_\mu > 0.2\%$, steady suction becomes more effective than oscillatory excitation in controlling the C_m. The form drag is initially increased by the excitation, in a comparable manner to the effect of weak suction, but for greater C_μ the effects of oscillatory excitation and steady suction are comparable. Steady blowing is inferior to oscillatory excitation over the entire $\langle c_\mu \rangle$ range that was available. It is concluded that the advantage of periodic excitation over steady boundary-layer control methods could be realized at a low $\langle c_\mu \rangle$ range, that is, $\langle c_\mu \rangle < 0.1\%$. The effect of the excitation frequency on the controlled integral parameters is weak, as could be inferred from the data, due to the two excitation frequencies that are presented in Fig. 15. (Note the agreement at the overlap region of the two frequencies.) Note that the model geometry was designed to be controlled by steady suction, and a design tool that properly utilizes periodic excitation is still missing.

IV. Conclusions

Active separation control was studied over a carefully documented baseline flow at high Reynolds numbers. The boundary layer on the model was turbulent throughout, so that laminar-turbulent transition does not baffle the data trends due to the active separation control. Indeed, the Reynolds number has a very weak effect on the model pressures. Even a reduction of 43% in the boundary-layer momentum thickness upstream of the model LE had a minor effect on the baseline separation and its control, indicating that Reynolds number R_θ is not a relevant parameter. The spanwise uniformity of the wall pressures was found to be very good and improved with control activated. The peak of the wall pressure fluctuations increased as reattachment moved forward due to control, regardless of the control method. Steady suction or blowing with a momentum coefficient of 2 to 4% was required to fully reattach the flow to the model and recover the ideal pressure distribution. Active control using periodic excitation was compared to steady mass flux and found to be of similar effectiveness as steady suction and significantly more effective than steady blowing. It was found that the superposition of weak suction on the periodic excitation enhances the receptivity of the separated shear layer to the fundamental excitation frequency and the effectiveness of the control method, whereas blowing promotes the generation of higher harmonics that are less effective. The experimental database presents a proper validation case for numerical simulation of unsteady flow control at high Reynolds numbers. This is because the boundary layers upstream and downstream of the model were not affected by the steady or unsteady separation control.

Acknowledgments

This work was performed while the first author held a National Research Council—NASA Langley Research Center Research Associateship. The authors would like to thank the following for their substantial support of the research program: W. L. Sellers III;

M. J. Walsh; R. D. Joslin; R. W. Wlezien; J. F. Barthelemy; A. McGowan, Manager, Aircraft Morphing program, Airframe Systems; B. L. Berrier; L. D. Leavitt; B. K. Stewart; G. C. Hilton; M. K. Chambers; L. Harris Jr.; P. I. Tiemsin; J. R. Knutson; P. T. Bauer; J. Thibodeaux; S. G. Flechner; J. T. Kegelman; S. P. Wilkinson; A. Bertelrud; and many other NASA employees and contractors.

References

[1]Betz, A., "History of Boundary Layer Control in Germany," *Boundary Layer and Flow Control*, Vol. 1, edited by G. V. Lachmann, Pergamon, Oxford, 1961, p. 2.

[2]Stratford, B. S., "An Experimental Flow with Zero Skin-Friction Throughout Its Region of Pressure Rise," *Journal of Fluid Mechanics*, Vol. 5, 1959, pp. 17–35.

[3]Goldschmied, F. R., "Approach to Turbulent Incompressible Separation Under Adverse Pressure Gradients," *Journal of Aircraft*, Vol. 2, No. 2, 1965, pp. 108–115.

[4]Liebeck, R. H., "Optimization of Airfoils for Maximum Lift," Ph.D. Dissertation, Dept. of Aeronautical and Astronautical Engineering, Univ. of Illinois, Urbana, IL, 1968.

[5]Lighthill, M. J., "A New Method of Two-Dimensional Aerodynamic Design," Aeronautical Research Council, R&M 2112, April 1945.

[6]Glauert, M. B., "The Design of Suction Aerofoils with a Very Large C_L-Range," Aeronautical Research Council, R&M 2111, Nov. 1945.

[7]Saeed, F., and Selig, M. S., "Multipoint Inverse Airfoil Design Method of Slot-Suction Airfoils," *Journal of Aircraft*, Vol. 33, No. 4, 1996, pp. 708–715.

[8]Glauert, M. B., Walker, W. S., Raymer, W. G., and Gregory, N., "Wind-Tunnel Tests on a Thick Suction Aerofoil with a Single Slot," Aeronautical Research Council, R&M 2646, Oct. 1948.

[9]Goldschmied, F. R., "Airfoil Static-Pressure Thrust: Flight-Test Verification," AIAA Aircraft Design and Operations Meeting, 1988.

[10]Goldschmied, F. R., "Integrated Hull Design, Boundary-Layer Control, and Propulsion of Submerged Bodies," *Journal of Hydronautics*, Vol. 1, No. 1, 1967, pp. 2–11.

[11]Nishri, B., and Wygnanski, I., "Effect of Periodic Excitation on Turbulent Flow Separation from a Flap," *AIAA Journal*, Vol. 36, No. 4, 1998, pp. 547–556.

[12]Seifert, A., Bachar, T., Koss, D., Shepshelovich, M., and Wygnanski, I., "Oscillatory Blowing, A Tool to Delay Boundary-Layer Separation," *AIAA Journal*, Vol. 31, No. 11, 1993, pp. 2052–2060.

[13]Seifert, A., Darabi, A., and Wygnanski, I., "Delay of Airfoil Stall by Periodic Excitation," *Journal of Aircraft*, Vol. 33, No. 4, 1996, pp. 691–699.

[14]Seifert, A., and Pack, L. G., "Oscillatory Control of Separation at High Reynolds Numbers," *AIAA Journal*, Vol. 37, No. 9, 1999, pp. 1062–1071.

[15]Rumsey, C. L., Gatski, T. B., Ying, S. X., and Bertelrud, A., "Prediction of High-Lift Flows Using Turbulent Closure Models," *AIAA Journal*, Vol. 36, No. 5, 1998, pp. 765–774.

[16]Goldschmied, F. R., "Fuselage Self-Propulsion by Static-Pressure Thrust: Wind-Tunnel Verification," AIAA Paper 87-2935, 1987.

[17]Seifert, A., and Pack, L. G., "Oscillatory Control of Shock-Induced Separation" *Journal of Aircraft*, Vol. 38, No. 3, 2001, pp. 464–472.

[18]Seifert, A., and Pack, L. G., "Sweep and Compressibility Effects on Separation Control at High Reynolds Numbers," AIAA Paper 2000-0410, Jan. 2000.

[19]Murthy, A. V., Johnson, C. B., Ray, E. J., Lawing, P. L., Thibodeaux, J. L., "Studies of Sidewall Boundary Layer in the Langley 0.3-Meter Transonic Cryogenic Tunnel With and Without Suction," NASA TP-2096, 1983.

[20]Ladson, C. A., and Ray, E. J., "Evolution, Calibration, and Operational Characteristics of the Two-Dimensional Test Section of the Langley 0.3-Meter Transonic Cryogenic Tunnel," NASA TP-2749, 1987.

[21]Rallo, R. A., Dress, D. A., and Siegle, H. J. A., "Operating Envelope Charts for the Langley 0.3-Meter Transonic Cryogenic Wind Tunnel," NASA TM-89008, 1986.

[22]Seifert, A., and Pack, L. G., "Oscillatory Control of Separation at High Reynolds Numbers," AIAA Paper 98-0214, Jan. 1998.

[23]Seifert, A., and Pack, L. G., "Active Control of Separated Flows on Generic Configurations at High Reynolds Numbers (Invited)," AIAA Paper 99-3403, June 1999.

[24]Heenan, A. F., and Morrison, J. F., "Passive Control of Pressure Fluctuations Generated by Separated Flow," *AIAA Journal*, Vol. 36, No. 6, 1998, pp. 1014–1022.

[25]Pack, L. G., and Seifert, A., "Dynamics of Active Separation Control at High Reynolds Numbers," AIAA Paper 2000-0409, Jan. 2000.

[26]Huerre, P., and Monkewitz, P. A., "Absolute and Convective Instabilities in Free Shear Layers," *Journal of Fluid Mechanics*, Vol. 159, 1985, pp. 151–168.

P. R. Bandyopadhyay
Associate Editor